Holocene sediments from the Southern Chile Trench: a record of active margin magmatism, tectonics and palaeoseismicity

Bianca Heberer, Georg Röser, Jan H. Behrmann, Meinert Rahn and Achim Kopf

Journal of the Geological Society 2010; v. 167; p. 539-553
doi:10.1144/0016-76492009-015

Journal of the Geological Society, London, Vol. **167**, 2010, pp. 539–553. doi: 10.1144/0016-76492009-015.

Holocene sediments from the Southern Chile Trench: a record of active margin magmatism, tectonics and palaeoseismicity

BIANCA HEBERER[1]*, GEORG RÖSER[2], JAN H. BEHRMANN[3], MEINERT RAHN[4] & ACHIM KOPF[5]

[1]*Department of Geography and Geology, University of Salzburg, Hellbrunner Strasse 34, 5020 Salzburg, Austria*

[2]*Anders Estenstads Veg 22, 7046 Trondheim, Norway*

[3]*IFM-GEOMAR, Wischofstrasse 1–3, 24148 Kiel, Germany*

[4]*ENSI, 5232 Villigen-ENSI, Switzerland*

[5]*RCOM, Universität Bremen, Leobener Strasse, 28539 Bremen, Germany*

**Corresponding author (e-mail: bianca.heberer@sbg.ac.at)*

Abstract: Sedimentology, petrography and the provenance of Holocene sediments from the Southern Chile Trench (36–47°S) were investigated in an integrated approach combining description of a collection of gravity cores, measurements of physical properties, quantitative X-ray petrography and modal analysis. The sediments studied were trench hemipelagic sediments, fan deposits, and more distal hemipelagic sediments from the Nazca Plate. The trench is mostly fed by multiple point sources via submarine canyons. Sandy turbidites show a southward increase in sediment maturity. Whereas volcanic lithic fragments and plagioclase represent the dominant fraction in the north, quartz content strongly increases in the southern part of the study area, in line with source lithologies. Further north, active volcanoes in the Main Cordillera represent almost the entire provenance signal as a result of a strong contribution of highly erodible volcanic rocks. Recurrence rates of sandy and silty turbidites in the trench fan sediments indicate a link to the palaeoseismic record on land. Our study documents the potential usefulness of proximal turbidites to reconstruct palaeoseismicity, even at a scale of single segments of the plate boundary.

Sedimentary fills of deep-sea trenches are sensitive recorders of long-term tectonics, shorter-term changes in surface processes, and even seismic cycles operating on very short (centennial) geological time scales at active plate margins. Whereas upper plate denudation, trenchward sediment transport, eventual subduction of sediments and involvement in generation of arc melts may be viewed as part of a more or less continuously operating cycle of solids and volatiles (e.g. Kilian & Behrmann 2003), the impacts of singular or cyclic events may also be documented in deep-sea trench sedimentation patterns and facies. This has been shown for cyclic changes of the global climate (e.g. Völker *et al*. 2006), regional climate (e.g. Lamy *et al*. 2001), deglaciation (e.g. Hebbeln *et al*. 2007) or even cycles of plate margin seismicity (e.g. Huh *et al*. 2004; Goldfinger *et al*. 2007). Mostly, this evidence has been collected from long-term stratigraphic records supported by one or a few drill-holes. We lack, however, more comprehensive investigations on the regional variations of sediment composition and dynamics within a single time slice in a deep-sea trench environment. Such studies would concern the character of the dispersed hemipelagic sedimentation, and would also refer to the turbidite record as a proxy for seismic activity, and to the provenance signal from the denudation area. Climate zones, large coseismic ruptures and major geological provinces on land are typically hundreds to about a thousand kilometres in size, and studies must, therefore, attempt to take this scale into account.

For a study of young sediments at this scale, we have chosen the Southern Chile Trench between 36° and 47°S latitude. In this paper we present a new set of sedimentological and petrographical data derived from the analysis of 16 gravity cores that were collected during R.V. *Sonne* expedition 181 (see Flüh & Grevemeyer 2005) from the Southern Chile Trench fill, from the hemipelagic sediments on the incoming Nazca Plate, and from trench fans formed at the mouths of submarine canyons seaward of major river systems on land. We specifically analysed grain-size distributions of the sediments, the mineralogy of fine-grained background sediments, the frequencies and petrography of the turbidites, and their provenance signal.

Plate-tectonic, oceanographic and climatic setting

The Southern Chile Trench relates to the subduction of the Nazca and Antarctic Plates beneath the South American Plate (Fig. 1). The most striking tectonic feature of the area is the subduction of an active spreading centre, the Chile Ridge, at about 46.4°S, 75.7°W (e.g. Behrmann *et al*. 1994), forming the Chile Triple Junction. Whereas the Nazca Plate is currently being subducted at about 6.6 cm a^{-1} (Angermann *et al*. 1999), faster rates prevailed over the past few million years, with maximum rates of up to 15 cm a^{-1} between 28 and 26 Ma (e.g. Angermann *et al*. 1999; Kendrick *et al*. 2003). The Antarctic Plate is subducted much more slowly at about 1.8 cm a^{-1} (DeMets *et al*. 1990). The oceanic crust that is currently subducted becomes progressively older northward and southward of the Chile Triple Junction. At the Nazca–South American plate boundary crustal ages range from zero to 33 Ma at about 36°S (e.g. Tebbens & Cande 1997). As a result, the thermal state varies and leads to a latitudinally different buoyancy of the subducted Nazca Plate, which contributes, along with the decreasing sediment input at lower latitudes, to the northward increasing water depth at the trench axis. Values range from *c*. 8200 mbsl (metres below sea

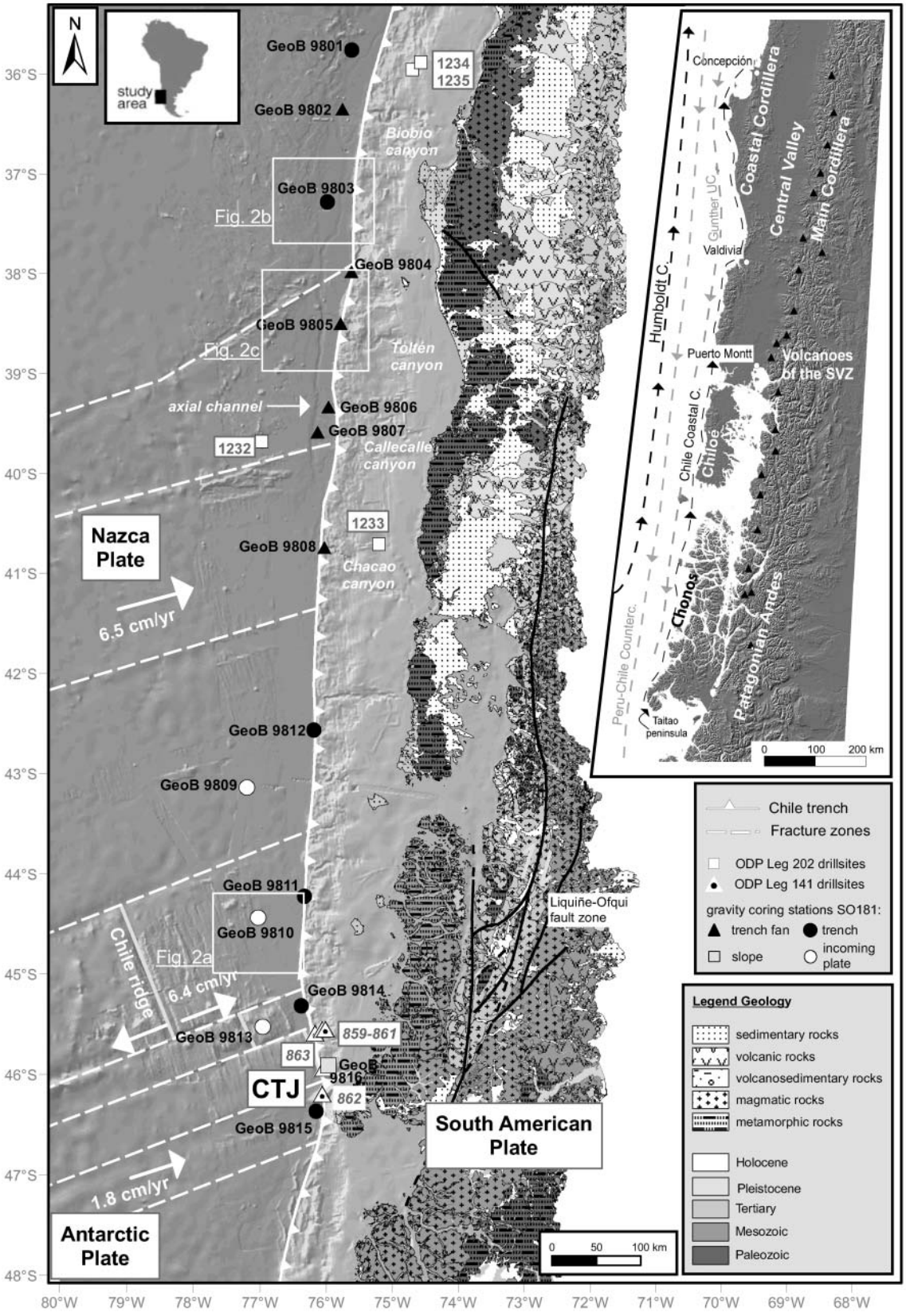

Fig. 1. Plate-tectonic, geological and bathymetric setting of the south–central Chilean margin including marine sampling sites. Inset shows main morphostructural units, active volcanoes and the offshore current pattern. Geology modified after SERNAGEOMIN (2003); bathymetry from Smith & Sandwell (1997).

level) off northern Chile (at 23°20'S) to around 4100 mbsl at 44°S and 3300 mbsl at the Chile Triple Junction (Smith & Sandwell 1997; Lindquist *et al*. 2004). Height differences of up to 15 km from the highest Andean peaks to the deepest parts in the trench (e.g. Galli-Olivier 1969; Scholl *et al*. 1970) mark the maximum height gradient on Earth.

The morphological structure of the trench changes radically from north to south. North of 32°S east–west cross-sections of the trench exhibit a U-shape, which changes southward to an asymmetrical V-shape, with a thick trench fill south of the Juan Fernandez Ridge, which blocks sediment transport to the north (Yañez *et al*. 2002; Ranero *et al*. 2006). South of 42°S the crustal structure of the trench is completely buried by sediments and is no longer detectable as a topographic feature (Lamy *et al*. 1998; Völker *et al*. 2006). Recent multibeam bathymetry data show that at *c*. 45°S the trench becomes a topographical trough again because of the increasing buoyancy of the young and hot oceanic plate in the vicinity of the Chile Triple Junction (e.g. Flüh & Grevemeyer 2005; Ranero *et al*. 2006). The average inclination of the continental slope is between 2.5° and 4.0° (Zapata 2001) and its width ranges from 50 to 80 km. It becomes steeper (10–15°) towards the trench floor (Scholl *et al*. 1970) and is steepest close to the Chile Triple Junction, where subduction erosion occurs (e.g. Behrmann & Kopf 2001). The continental slope is irregular in shape, showing small plateaux, lineaments, and escarpments (Fig. 2; see also Zapata 2001; Ranero *et al*. 2006). Between 41°S and 36°S five major submarine canyons dissect the slope: the Chacao, Callecalle, Toltén, Imperial, and Biobío canyons (Fig. 1; see also Thornburg *et al*. 1990; Völker *et al*. 2006). North of 36°S, there is a number of smaller unnamed canyons and the large San Antonio Canyon off Valparaiso (Laursen & Normark 2002). Most of the bending in the Nazca Plate and associated formation of horst and graben structures is located in a narrow zone near the outer edge of the trench (Fig. 2b; see also Flüh & Grevemeyer 2005).

The oceanographic setting is described briefly here as it plays an important role in sediment transport and distribution off Southern Chile. Reviews of the topic have been given by Shaffer *et al*. (1995) and Strub *et al*. (1998), and a more recent report of the Holocene–Pleistocene palaeoceanographic record in the cores of Ocean Drilling Program (ODP) Sites 1232 and 1233, located at about 40°S, has been given by Mix *et al*. (2003). The eastward-directed Antarctic Circumpolar Current reaches the Chilean coast at *c*. 45°S, where it splits into the southward Cape Horn Current (Boltovskoy 1976) and the northward flowing Humboldt Current. Parallel to the Humboldt Current, the poleward Peru–Chile Countercurrent transports subtropical surface water to the south. Near the coast the Chile Coastal Current flows northward (Strub *et al*. 1998). Over the continental slope and outer shelf, the Gunther Undercurrent transports equatorial subsurface water to the south at water depths between 400 and 1200 mbsl (Fig. 1).

Erosion, fluvial transport and thus sedimentation are directly related to precipitation rates, which show a pronounced latitudinal zonation along the western, windward side of the Andean orogen of Chile, ranging from the hyperarid Atacama Desert in the north to a region of very high rainfall in the Patagonian Andes in the south. The study area does not include these two extremes, but it does cover highly variable segments of the orogen with rivers as the prime agent for moving sediment from the continental source to the slope and trench. In the central part of Chile between 31 and 38°S, climate can be classified as semiarid Mediterranean, reflected in an increased river density

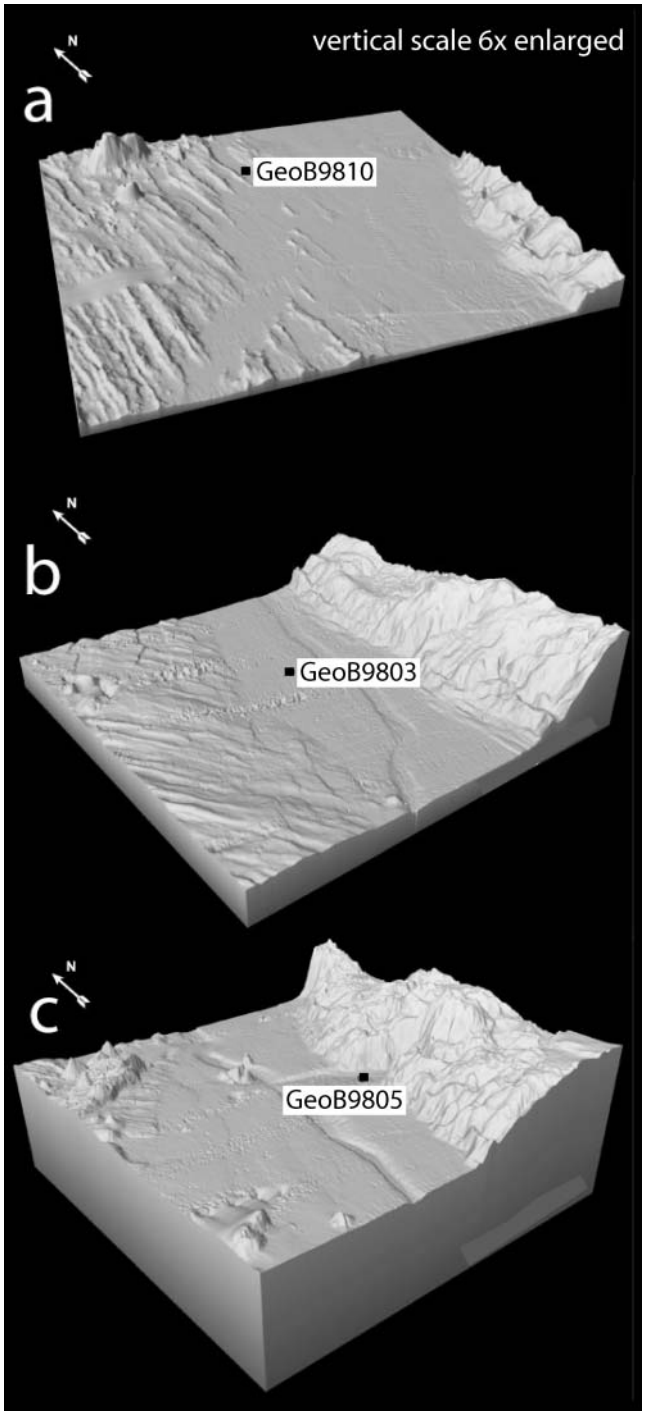

Fig. 2. Block diagrams of the main sampling sites: (**a**) incoming plate; (**b**) trench fill; (**c**) trench fan (Toltén fan). Horst and graben structures have developed as a result of the downbending of the Nazca Plate (**a**). South of 41°S turbidity currents may travel across the trench (**a**), whereas north of this latitude they are diverted northwards along the axial channel (**b**, **c**).

and much higher fluvial supply than north of these latitudes (Lamy *et al*. 1998). Precipitation varies from 300 to around 1000 mm a^{-1}, increasing to the south. At 38°S a major discontinuity in annual rainfall is present, as a result of the northernmost reaches of the southern westerlies at this latitude, with summer dryness disappearing in the central–southern part

of Chile (38 and 42°S). The climate is rainy–temperate with annual rainfall in the range 1000–2000 mm a^{-1} at low elevations and even higher values in the Andes (Lamy *et al*. 1998, and references therein; Sepúlveda *et al*. 2006). Precipitation rates further increase in the Patagonian Andes, with maximum values as high as 5000 mm a^{-1} south of the study area at *c*. 50°S forcing intense erosion that transports voluminous clastic debris westward to the offshore trench. Besides the marked latitudinal zonation, rainfall also varies longitudinally as a result of the orographic rise of moist air masses. For the Biobío drainage, for example, average annual rates are 2300 mm, but values range from 1100 mm in coastal areas to almost 5000 mm at the high altitudes of the Main Cordillera (Link *et al*. 2002). Major rivers, such as the 380 km long Biobío, drain all three major morpho-structural units.

Sedimentation in the Southern Chile Trench

Sediments of the Southern Chile Trench are mainly composed of olive green to olive grey hemipelagic clayey silt to silty clay, intercalated with frequent sandy turbidite layers that are dark grey to black (Fig. 3; e.g. Behrmann *et al*. 1992; Lamy *et al*. 1998; Hebbeln *et al*. 2001; Flüh & Grevemeyer 2005; Sick *et al*. 2006; Blumberg *et al*. 2008). North of 41°S, turbidity currents emanate from multiple point sources, which correspond to major river systems draining the western side of the Andean orogen. These rivers continue their paths across the shelf and the continental slope via submarine canyons to build submarine fans at the trench floor, which extend seaward across the trench basin. High river discharge and focused transport of eroded material within these canyon systems have led to a huge amount of

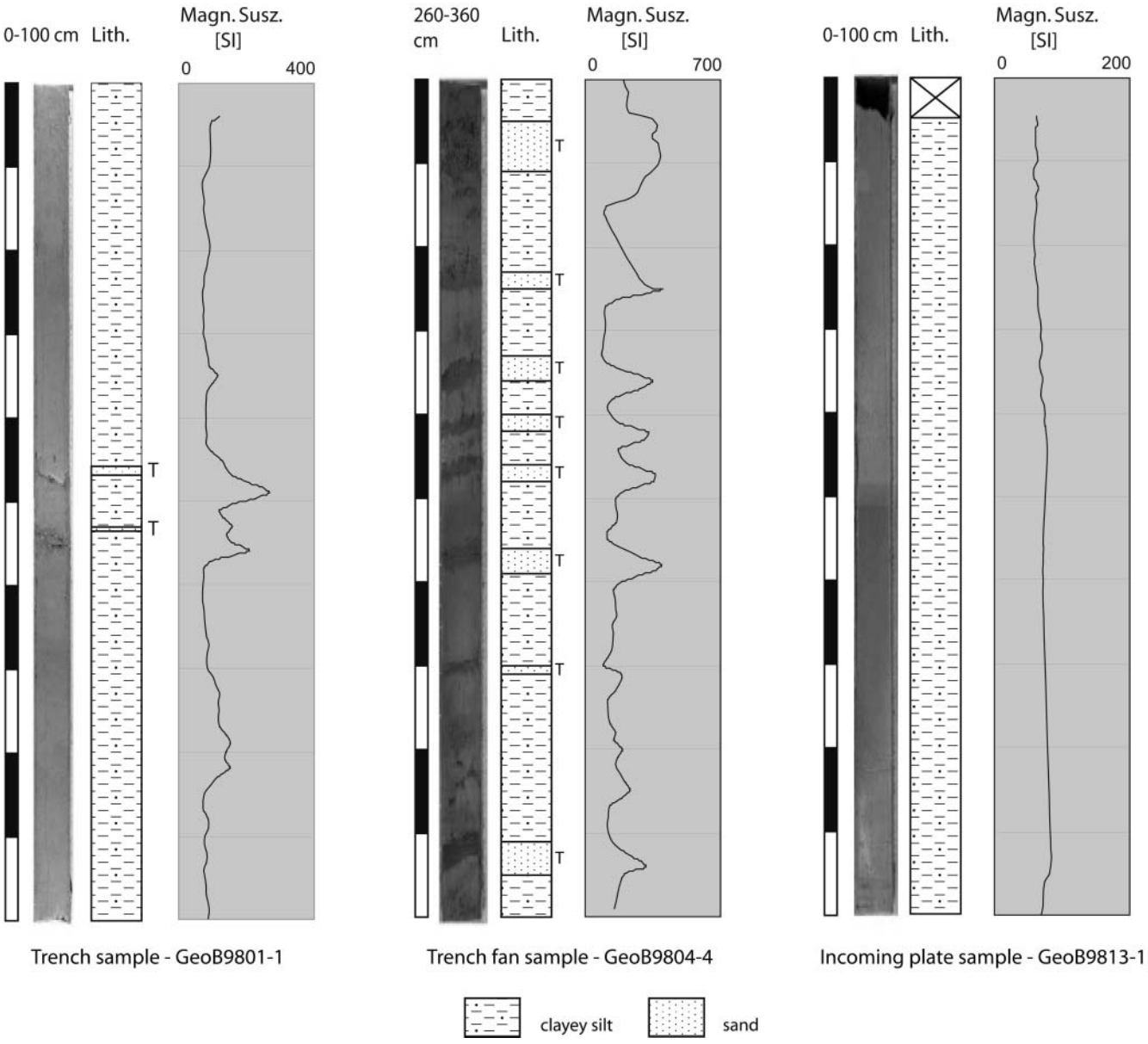

Fig. 3. Representative gravity cores for trench, trench fan and incoming plate sampling sites. Turbiditic layers (T) occur at high frequency within the proximal trench fan sections, but are almost absent within the distal sites of the incoming plate.

particles being transported to the trench fans and trench. In addition, margin-parallel currents play an important role in funnelling further sediment into the canyons. At 40°S, strong shelf currents carry fine-grained material to the canyons, which is then channelled downslope to the deep sea (Hebbeln *et al*. 2001). ODP Site 1232 (Mix *et al*. 2003), located on the Nazca Plate seaward of the Chile Trench (Fig. 1), revealed a 0.46–0.78 Ma long record of hemipelagic sedimentation interrupted by distal turbidites, suggesting a centennial frequency in turbidite activity.

South of 41°S, sediment transport is more complex because of the rugged fjordland topography, the drowned forearc basin, the dissection into a multitude of islands, and a very wide shelf (up to 150 km, Scholl *et al*. 1970; Fig. 1). Drainage systems are much smaller, and source and sink cannot be as easily linked as for the central segment of the study area. Turbidite thickness and frequency is expected to vary according to the proximity to the source (i.e. submarine canyons and oversteepened slopes).

The 2–3 km thick sediment fill of the trench has a wedge shape, onlapping the pelagic sediment cover of the Nazca Plate. Between about 41°S and 30°S sediment in the trench is transported northward along a slightly inclined axial channel (e.g. Scholl *et al*. 1970; Thornburg & Kulm 1987*a*,*b*; Laursen & Normark 2002), which cuts up to 200 m into the trench sediments (Figs 1 and 2b). This marks a change in the depositional system, as south of 41°S sheet turbidites may cross the entire width of the trench, but north of this latitude they are partially diverted northward following a longitudinal transport (Thornburg & Kulm 1987*b*). The general northward direction of sediment transport is underlined by the asymmetry of trench fan deposits (Thornburg *et al*. 1990; Völker *et al*. 2006) and the distribution pattern of the axial sediment fill (Schweller & Kulm 1978). Similar systems seem to operate in other modern arc–trench systems, and have been described for the Middle America Trench (Underwood & Karig 1980) and the Nankai Trench (e.g. Underwood *et al*. 1993; Bangs *et al*. 1999). It is assumed that this tectonic framework did not undergo major changes since the latest Neogene, and the structural information from seismic data can be used for the spatial definition of the depositional system.

The continental sediment source

Because of the short transport distances between sediment sources in the Andes and the Coastal Cordillera on the one hand, and the system of multiple river drainages on the other, the Southern Chile Trench is well suited to relate sediment source and sink, to document latitudinal variations in composition and provenance, and thus to test the homogenizing effect of longitudinal sediment dispersal parallel to the trench axis. A comprehensive overview of the onland geology of Chile has been given by Moreno & Gibbons (2007). The study area is divided into three parallel geomorphological zones: the basement high of the Coastal Cordillera, with elevations up to 1500 m; the Central Depression (or Longitudinal Valley); and the Main Cordillera, with heights of more than 6000 m (Fig. 1).

Between 33°S and 38°S, the Coastal Cordillera is dominated by intrusive rocks of Palaeozoic to early Mesozoic age (e.g. Melnick & Echtler 2006). South of this latitude, metasediments prevail. Two lithological units, the Western and the Eastern Series, are distinguished, representing a pre-Andean paired metamophic belt (Aguirre *et al*. 1972). The Western Series is interpreted as the basal part of a Permotriassic accretionary wedge, which developed along the SE margin of Gondwana (Aguirre *et al*. 1972), whereas the Eastern Series represents a Carboniferous–Permian magmatic arc (Martin *et al*. 1999; Willner *et al*. 2000).

The Central Depression represents a forearc alluvial basin, filled with a thick succession of Mesozoic to Quaternary continental clastic and volcanoclastic sediments, derived from the Main Cordillera (Pankhurst & Hervé 2007). South of 33°S, the Central Depression is filled with up to 4000 m of alluvial sediment of Quaternary age (LeRoux & Elgueta 2000; Melnick & Echtler 2006). South of Puerto Montt (41°S), the sediment surface of the Central Depression subsides below sea level.

In the Main Cordillera between 33°S and 46°S, a Pliocene to modern active volcanic arc (the Southern Volcanic Zone) developed above a basement that is mainly composed of an eroded Late Jurassic to Miocene magmatic arc. South of 46°S, active volcanism is absent and this volcanic gap, which has been correlated with the subduction of the Chile Ridge (e.g. Ramos & Kay 1992), stretches 350 km south to the Austral Volcanic Zone. Landward of the Chile Triple Junction, calcalkaline rocks of the North Patagonian Batholith, which forms large parts of the Southern Chilean Andes, predominate (e.g. Melnick & Echtler 2006).

Sampling sites and methods

Sixteen gravity cores were recovered between 36°S and 47°S (Fig. 1) off southern Chile (see Flüh & Grevemeyer 2005) during R.V. *Sonne* Cruise 181 (December 2004 to January 2005), which was part of the research campaign TIPTEQ. Exact locations for coring were determined on the basis of pre-existing bathymetric data and from data collected by the multibeam bathymetric SIMRAD system EM120 and a Parasound 3.5 kHz system installed aboard R.V. *Sonne*. Cores were cut into 1 m long sections, which are stored at the University of Bremen, in the IODP Core Repository. No age dating was carried out on the cores, but because of high sedimentation rates and short core lengths a Holocene age can be inferred (see discussion below for details).

Mainly three depositional settings were targeted for gravity coring: the trench fill (Cores GeoB9801, -03, -11, -12, -14, and -15), deep-sea trench fans (GeoB9802 and GeoB9804 to -08) and the incoming oceanic Nazca Plate (GeoB9809, -13 and -10). An additional core comes from the continental slope near the Chile Triple Junction (GeoB9816). Core GeoB9810 was sampled in an area where deformation of the incoming plate as a result of downbending occurs (Fig. 2). Prominent horst and graben structures, covered by pelagic sediments, can be seen (Fig. 2a). One core, GeoB9816, was taken on the continental slope at 1522 m, in the hanging wall of a large normal fault that was first described by Behrmann *et al*. (1992). A detailed description of the gravity cores and documentation of the core-related database has been given by Röser (2007). Table 1 gives an overview of the parameters discussed below.

Water depth at the sampling localities decreases southwards as a result of a higher sediment supply and decreasing ocean floor ages. When testing core material with hydrochloric acid, we found sediment containing detectable carbonate in cores to about 4300 m water depth, and no carbonate in cores located 200 m deeper, in agreement with Hebbeln *et al*. (2007), who placed the carbonate compensation depth (CCD) off Southern Chile at 4500 m. Thus the transition from sampling sites below the CCD to those above the CCD is located at *c*. 41°S.

Grain-size analysis

Grain-size analyses of hemipelagic and turbiditic material were carried out for all cores at Bremen University (Harbers 2005).

Table 1. *Summary of locations and measured core parameters of SO181 gravity cores*

Core number	Latitude (°S)	Longitude (°W)	Water depth (m)	Location	Length (cm)	Turbidite quantity	Turbidites m^{-1}	Average turbidite thickness (cm)	Background sediment (%)	Average turbidite recurrence rate (years) (arithmetic mean)	Average turbidite recurrence rate (years) (median)	Recurrence rate minimum (years)	Recurrence rate maximum (years)
GeoB9801	35°59.991′	74°25.054′	4934	Chile Trench	500	14	2.80	2.07	94.2				
GeoB9802	36°35.001′	74°35.001′	4822	Biobio TF	170	8	4.71	3.19	85.0	218 ± 117	153	109	447
GeoB9803	37°30.304′	74°50.353′	4679	Chile Trench	650	1	0.15	5.00	99.2				
GeoB9804	38°14.999′	74°35.494′	4606	Imperial TF	460	32	7.17	2.38	82.9	192 ± 146	152	32	620
GeoB9805	38°45.049′	74°46.134′	4513	Toltén TF	240	7	2.92	3.57	89.6	327 ± 346	201	81	1086
GeoB9806	39°34.971′	75°00.000′	4293	Callecalle TF	500	22	4.40	1.91	91.6	334 ± 338	195	76	1413
GeoB9807	39°50.075′	75°00.104′	4300	Callecalle TF	700	22	3.14	2.57	91.9	477 ± 274	463	131	1468
GeoB9808	41°00.001′	75°11.093′	3905	Chacao TF	585	31	5.30	5.19	72.5	240 ± 105	272	22	468
GeoB9809	43°21.254′	76°29.510′	3504	Nazca Plate	275	1	0.36	3.00	98.9				
GeoB9810	44°40.044′	76°29.852′	3245	Nazca Plate	560	6	1.07	3.67	96.1				
GeoB9811	44°30.034′	75°49.871′	3324	Chile Trench	275	8	2.91	4.25	87.6				
GeoB9812	42°50.044′	75°30.005′	3700	Chile Trench	500	15	3.00	1.53	95.4				
GeoB9813	45°45.990′	76°35.004′	2689	Nazca Plate	500	0	0.00	0.00	100				
GeoB9814	45°36.005′	75°59.997′	3326	Chile Trench	400	19	4.75	3.18	84.9				
GeoB9815	46°40.161′	75°55.379′	3399	Chile Trench	235	0	0.00	0.00	100				
GeoB9816	46°13.019′	75°41.018′	1522	Continental slope	270	0	0.00	0.00	100				

TF, trench fan.

Hemipelagic background sediment was sampled at a constant spacing of 1 m. During visual core description smear slides were made for the turbiditic sections and one representative sample per core was chosen. Prior to grain-size analysis the samples were treated with 3.5% hydrogen peroxide (H_2O_2) to remove organic matter and with sodium pyrophosphate ($Na_4P_2O_7$) to inhibit coagulation of clay size particles. The >63 μm fraction was removed by sieving. Salt particles were dissolved by boiling the samples. A Beckmann Coulter LS 200 laser particle sizer with a detectable grain-size range from 0.4 to 2000 μm was used to measure grain sizes of particles in suspension (for details, see Moerz & Wolf-Welling 2002).

Physical properties

P-wave velocity, bulk density using gamma-ray attenuation and magnetic susceptibility were measured with a GEOTEK multi-sensor core logger. This is a powerful non-destructive device for continuous measurements of geophysical data on marine sediment cores. Measurements are automatically taken every centimetre and recorded electronically (e.g. Weber *et al*. 1996, 1997). A detailed documentation of the results and experimental procedures has been given by Röser (2007). Here we discuss the results for magnetic susceptibility. This is measured with a Bartington loop sensor (60–150 mm diameter) by exposing the core to an external magnetic field, in which the sediment becomes magnetized according to the amounts of iron-bearing minerals present within the sample. Because the end caps of each section produced unreliable data near the ends of each 1 m segment, these data points were removed.

After core logging, 10 cm^3 of homogeneous hemipelagic material from every second core metre were sampled for the analysis of wet bulk density. Samples were dried at 80 °C and then measured with a Quantachrome Pentapycnometer (Harbers 2005), which gives a single-measurement accuracy between 0.02 and 0.03%.

Bulk mineralogy

X-ray diffraction (XRD) analysis was carried out on material <63 μm from all cores of R.V. *Sonne* cruise SO181. Samples from the hemipelagic intervals, which had previously been tested for different geotechnical parameters (Röser 2007), were investigated. Therefore the number of measurements per core varies depending on the number of shear tests.

A Siemens D5000 diffractometer and the enclosed DIFFRAC^{plus} software package were used to measure and determine mineral phases. Quantitative phase analysis was based on the Rietveld method (Rietveld 1969) using BGMN/Auto-Quan®. Reflections between 3° and 6° 2θ were summarized as 'chlorite'.

Modal analysis

Modal analyses were carried out on 30 turbiditic samples found in most of the 16 gravity cores. Where present, one turbidite at the bottom, in the middle and in the top section of each core was sampled. Epoxy grain mounts from the sieved sand fractions were half etched and stained to differentiate K- and Na-rich feldspars (Marsaglia & Tazaki 1992). A total of 400 points were counted on each sample using an automatic point counter. The Gazzi–Dickinson method was applied to minimize uncertainties based on grain-size variations by counting mineral grains of sand size within larger rock fragments as the mineral concerned

instead of the fragment (Dickinson 1970). The counted components were divided into 30 compositional categories. A detailed account of the data has been given by Heberer (2008).

Results

Core description

Gravity cores from all sites are dominated by fine silt to clayey, olive green to grey hemipelagic background sediment, intercalated with variably frequent turbidites. The turbidites are dark grey to black, and are mainly composed of medium-grained sand. Erosional bases and occasional fining upward trends are observed. Representative cores for all sampling sites are shown in Figure 3. Major differences between the sites are found in the turbidite frequency, which is highest within the trench fans (average of 4.6 m^{-1}), decreases within the trench fill (2.3 m^{-1}) and is lowest on the incoming plate (0.5 m^{-1}) (Table 1). No such trend is observed for the average thickness of the turbidites, which is rather constant (3.1, 2.7 and 3.5 cm; Table 1), although the range varies, with maximum values of 18 cm for cores from trench fans. The grain size of the turbidites varies with proximity to the source, and thus is coarsest within the trench fans (mainly fine to medium sands) and decreases within the trench fill and on the incoming plate (mainly silt to fine sands).

Core GeoB9816 contains black layers and released an intense sulphuric smell when cut in half, and shows elevated amounts of decomposing pyrite on XRD analysis (Röser 2007), attesting to a low-oxygen sedimentary environment at this part of the continental slope. The uppermost core metre comprises silt to fine sand of olive-greyish colour. Further down-core black sandy layers are intercalated, followed by grey silty clay with two cobble-bearing horizons. These cobbles are interpreted as locally reworked indurated material from the footwall of the fault zone. Young fault movements have probably exposed Pleistocene deposits akin to those intersected at ODP Site 863 (see Fig. 1, and Behrmann *et al*. 1992), covered by a thin section of younger sediment.

Grain-size analysis

Within the background sediment, silt is the dominant size fraction in all cores, ranging from about 70 to 80% (Fig. 4a). Increasing clay contents are accompanied by decreasing sand contents irrespective of the tectono-sedimentary setting. Clay and sand size fractions do not vary much across the CCD, indicating that the sand- and silt-sized biogenic calcite component in the sediments is low. Higher sand fractions correlate with the vicinity of feeding river systems, as observed for all the trench fan sites between 36°S and 41°S, and for the southernmost coring stations GeoB9815 and -16 (Fig. 1), where the source areas on land are nearby. This is seen as a strong qualitative indicator of river input. The grain-size composition of cores from the segment of the Chilean margin south of 41°, where large river systems are absent, differs notably. Here, the sand size fraction falls below 10%, whereas the clay fraction rises to values between 18 and 24%. These differences are explained by differences in the geomorphology and drainage systems in the source area, but also by the proximity between source and sink. It further appears that homogenization of the hemipelagic sediment by trench-parallel redistribution may be less efficient than previously thought.

The turbidites (Fig. 4b) are dominated by fine sand, with variable contributions of silt-sized components. The trench fan turbidites contain generally more sand than those deposited in the trench, or on the Nazca Plate (Fig. 4b). Cores GeoB9813, -15 and -16 do not contain turbidites.

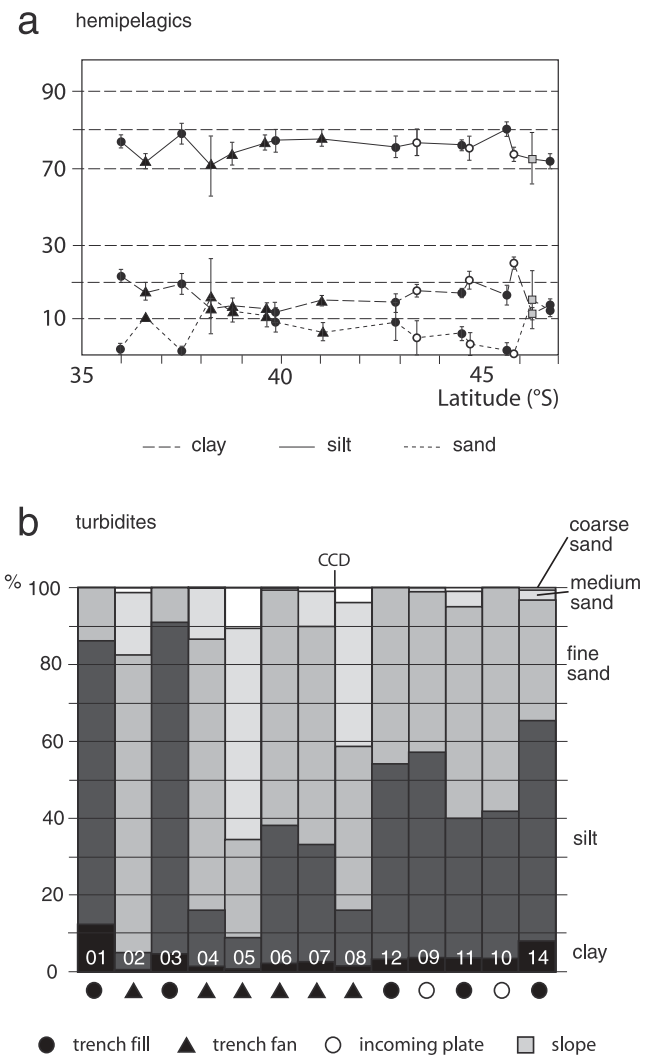

Fig. 4. Grain-size distributions of all SO181 gravity cores for the hemipelagic background sediment (**a**) and the turbiditic layers (**b**). Trench fan sites show elevated sand contents for both lithologies.

Physical properties

Magnetic susceptibility shows consistently higher values within the turbiditic layers as a result of elevated contents of iron-bearing volcanic lithic fragments in the sands, as shown by modal analyses. Maximum values are measured for the turbidites from trench fan deposits (Fig. 3). When averaged over the entire length of a single core (which ranges from 170 to 700 cm), the trench hemipelagic deposits show a range in magnetic susceptibilities of about (48–160) $\times$ 10^{-6} SI, whereas the trench fan averages are about (160–280) $\times$ 10^{-6} SI, and those of Nazca Plate sediments are about (90–120) $\times$ 10^{-6} SI (Fig. 5a). Because the trench fans with the highest values are located in the north of the study area, linear regression of the averaged data indicates a 50% northward increase from about 100 $\times$ 10^{-6} to 200 $\times$ 10^{-6} SI (Fig. 5a). The former value is similar to those recorded in near-surface sediments at the ODP Leg 141 drill sites (Fig. 1; Behrmann *et al*. 1992). The northward increase is a direct

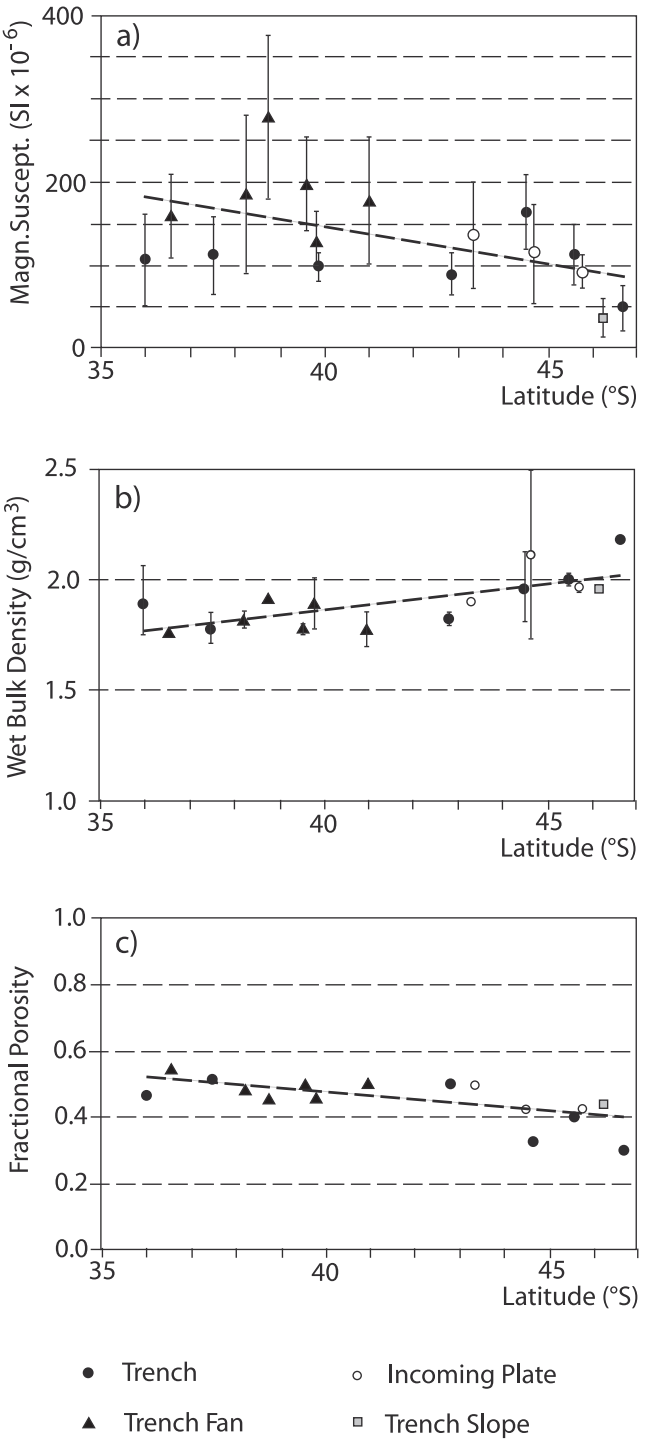

Fig. 5. Latitudinal variations of magnetic susceptibility (**a**), wet bulk density (**b**) and fractional porosity (**c**). Values are averaged over whole cores and error bars indicate one standard deviation. Southward decreasing magnetic susceptibility correlates with decreasing input of volcanic detritus into the trench. Slightly higher densities in the south may be caused by elevated clay contents.

reflection of higher input of fresh volcanic detritus via rivers into the trench fan systems.

The average wet bulk density value of all cores is 1.89 g cm^{-3}. Figure 5b shows the core-by-core variations of average wet bulk density with latitude. Linear regression of the data shows a slight north-to-south increase from 1.8 to about 2.0 g cm^{-3}. The higher densities in the south are tentatively related to elevated clay contents in the samples (see above). Fractional porosities were calculated from the density data assuming a grain density of 2.7 g cm^{-3}, leading to a inverse trend to that shown by the bulk density data (compare Fig. 5b and c) The total average for hemipelagic sediment from all cores is 0.46. This value is typical for silts with a low fraction of clay-sized particles, and is marginally lower than the porosities determined from silty near-surface sediments on the lower continental slope near the Chile Triple Junction (see Behrmann *et al*. 1992).

Bulk mineralogy of the hemipelagic sediments

Principal mineral phases and their latitudinal variations are given in Figure 6. Generally the most abundant phase is plagioclase, with average sample contents ranging from 27 to 54%. The highest concentrations are found in the north, and a pronounced north-to-south decrease is observed together with a gradual increase in quartz content from 8% to as much as 30%. K-feldspar is present in nearly all samples, with a local maximum of 6%. Calcite, mostly biogenic, is present in low concentrations in samples above the CCD (i.e. south of *c*. 41°S). Here, calcite contents range between about 2 and 9%. Values for plagioclase, quartz and calcite are similar to those at ODP Leg 141 (Behrmann *et al*. 1992) We interpret the trends observed for plagioclase and quartz to reflect differences in the large-scale geological picture on land, with abundant intermediate to mafic volcanic rocks in the north, and vast outcrops of intermediate to acid plutonic rocks of the Patagonian Batholith in the south (Fig. 1).

The combined abundances of illite and mica are between about 17 and 34%. A smaller part of these are assumed to be detrital white micas, and the remainder is probably a combination of fine-grained suspension fallout and products of pervasive plagioclase alteration and devitrification processes, as observed in the sand-sized fractions of the intercalated turbidites (see below). As found in most of the ODP Leg 141 cores (Behrmann *et al*. 1992), illite dominates over smectite in the analysed cores. The observed discrepancy between the total abundances of clay-sized particles in the hemipelagic sediments (10–25%; see Fig. 5a) and the abundance of clay minerals, chlorite and mica (24–44%; Fig. 7) is due to the fact that a substantial fraction of the sheet silicates is contained in altered feldspars and devitrified volcanic glass in the silt fraction (see also the description below for the sand-sized turbidites).

Additional detectable mineral phases identified by the Rietveld analysis are halite (1–2%, probably remaining from seawater after sample drying), detrital amphibole, and pyrite.

Modal analysis of turbidite layers

Shapes of sand grains range from very angular to rounded, but are commonly subangular to subrounded (Fig. 7a). Monomineralic grains are predominantly plagioclase and quartz, which is a first-order reflection of the mineral proportions found in the finer-grained hemipelagic background sediment (see the previous paragraph). Amphibole, pyroxene, K-feldspar and opaque minerals occur in small abundances in most of the samples. Zircon is the most frequent accessory component.

Monocrystalline quartz reveals both undulatory and non-undulatory extinction within grains from the same sample. Polycrystalline quartz is present in minor amounts in most of the samples, exhibiting both straight and sutured grain boundaries.

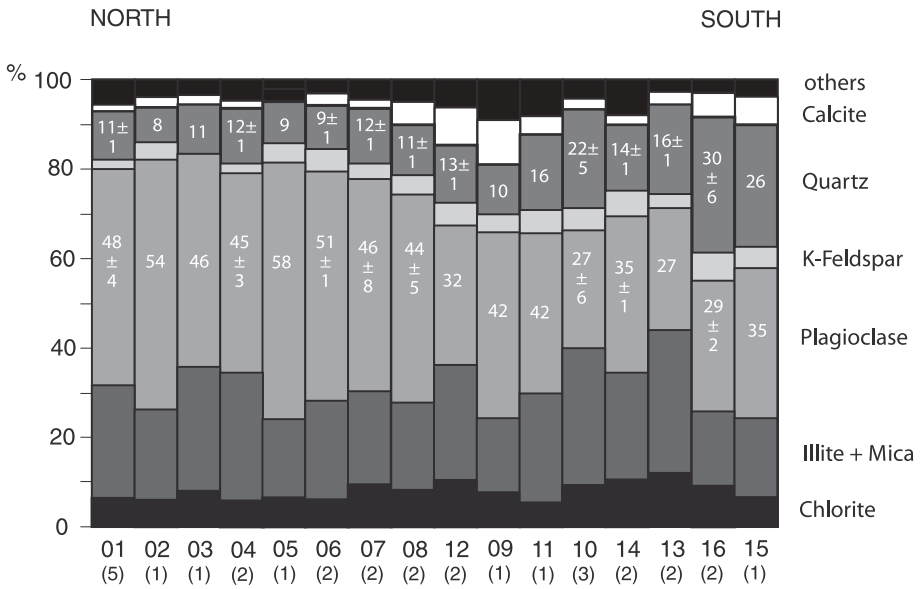

Fig. 6. Latitudinal variations of major mineral phases from XRD analysis on hemipelagic sections showing a prominent southward increase of quartz and reverse trend for plagioclase contents, in line with areally widespread volcanic rocks in northern and batholithic rocks in southern source areas. Percentages of quartz and feldspar are also given as an average value ± one standard deviation. Numbers in parentheses along the horizontal axis give the number of measurements for each core.

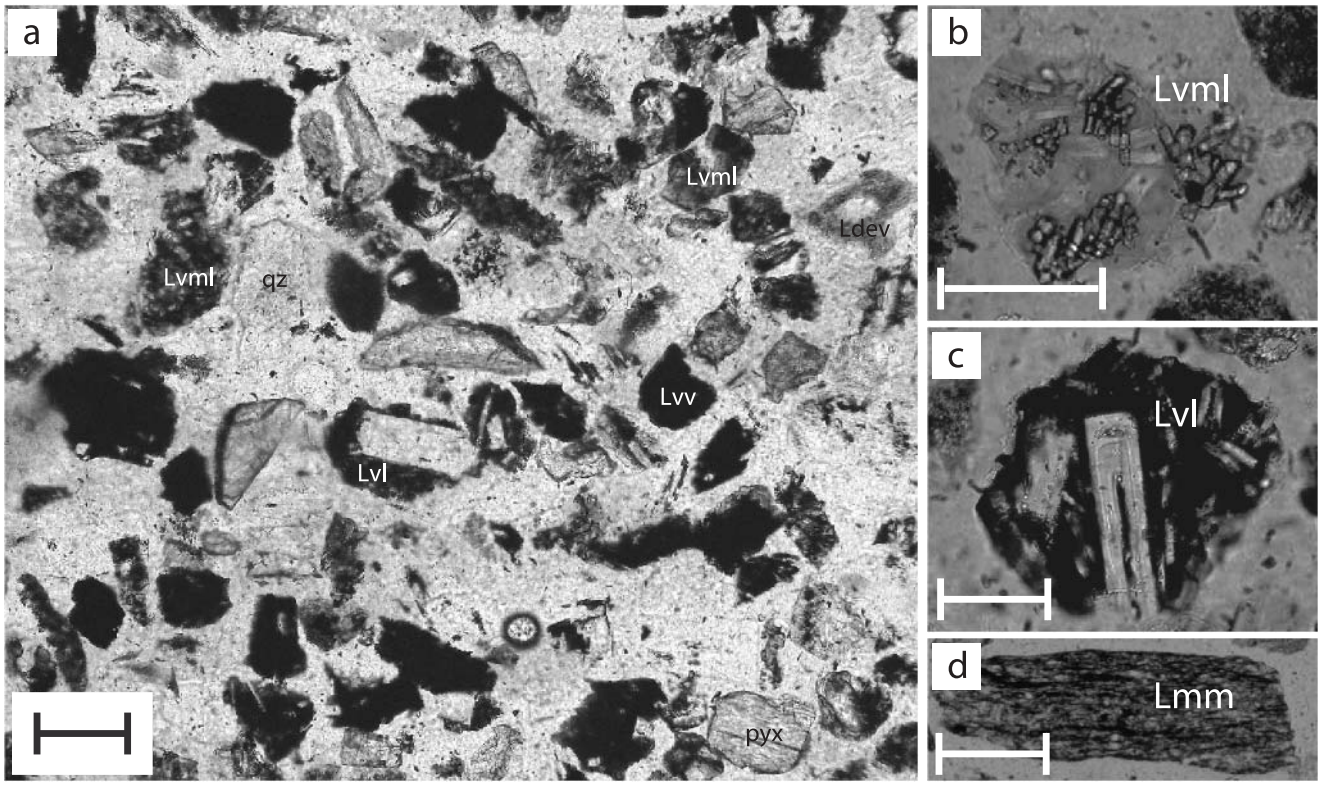

Fig. 7. Photomicrographs of unstained turbidite grain mounts under plane-polarized light. (**a**) Overview of a typical thin section, rich in mostly black or dark brown volcanic lithic fragments; (**b**) brown microlitic fragment (Lvml); (**c**) black lathwork grain (Lvl) with sand-sized feldspar; (**d**) metamorphic lithic fragment (Lmm) from the vicinity of the Chile Triple Junction. Scale bars represent 100 μm. Ldev, devitrified lithic.

Along with a general increase of the total amount of quartz towards the south, polycrystalline grains are rare in samples from the north and more frequent south of *c*. 44°S. This indicates a southward increasing proportion of detrital quartz derived from metamorphic rocks.

Plagioclase is the dominant feldspar in all samples, and its high abundance in the sands analysed is reflected in the two QFL diagrams in Figure 8a and b. The grains are variably affected by alteration, ranging from very fresh, albite-twinned grains to grains almost entirely altered to sericite and/or epidote. The latter have a cloudy appearance under the microscope in plane-polarized light. Strong feldspar alteration is usually associated with a higher proportion of devitrified volcanic lithic fragments. K-feldspar is rare.

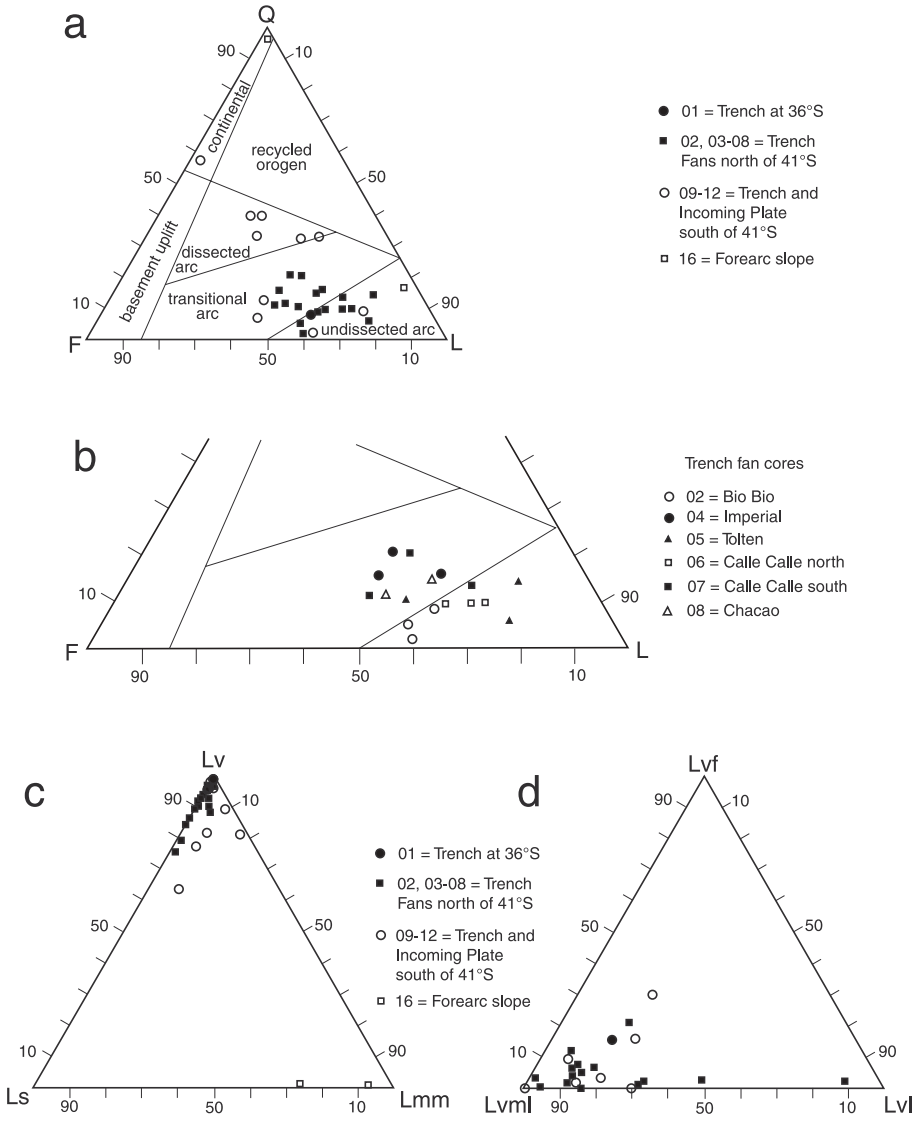

Fig. 8. Results from modal analysis on sand fractions from turbiditic layers after Dickinson (1970) (Q, quartz; F, feldspar; L, lithic fragment; Lv, Ls, Lmm, volcanic, sedimentary, metamorphic lithic fragment; Lvf, Lvml, Lvl, volcanic lithic fragment with felsic, microlitic and lathwork texture). All trench fan samples carry an 'undissected' or 'transitional arc' signature in a standard QFL diagram, whereas more southerly samples are more quartzose in nature (**a**). Samples from the Biobío fan show the strongest volcanic provenance signal (**b**). Apart from a few exceptions from the southernmost study area, rock fragments are mostly of volcanic origin (**c**) with microlitic textures (**d**), indicative of basaltic to basaltic andesite compositions.

Apart from a few exceptions in the southernmost part of the study area, volcanic lithic fragments (Lv) represent the dominant lithic fragment type in the core samples (Fig. 8c), and were distinguished according to their texture following Dickinson (1970). Abundant microlitic volcanic grains (Lvml) represent mostly intermediate lava types and include silt-sized feldspar laths and ferromagnesian minerals (Fig. 7a and b). Their groundmass is usually made up of black or brown glass, with frequent devitrification. In rare cases the ground mass is holocrystalline (pilotaxitic) and not glassy. Subordinate lathwork volcanic grains (Lvl) typically occur in basaltic to basaltic andesite lavas and pyroclastic rocks, and contain sand-sized plagioclase or pyroxene suspended in a vitric or devitrified groundmass (Fig. 7a and c) Furthermore, vitric volcanic grains (Lvv) without microlites were distinguished by their glass colour (Fig. 7a). They are generally brown, dark brown or black. Rare felsitic grains (Lvf) are composed of anhedral quartz and feldspar, forming a fine-grained mosaic characteristic of silicic volcanic rocks. All vitric fragments were further subdivided depending on their colour under the microscope in plane-polarized light. According to Schmincke (1982), a decrease in silica content is reflected by a darker glass colour. Most commonly opaque or dark brown tachylitic glass occurs, whereas the abundances of light brown sideromelane or transparent vitric fragments are negligibly small. Almost no bubble-wall fragments and vesicular glass were detected. Other volcanic fragments (conforming to the definition of Marsaglia *et al*. 1995) comprise holocrystalline aggregates of plagioclase, opaque phases and pyroxene.

The degree of devitrification of glassy fragments and alteration to clay minerals is generally high. Only in samples taken in the Biobío fan (core GeoB9802) are most glassy fragments fresh, largely angular and characterized by a higher grade of vesicularity. This suggests that they did not undergo extensive abrasive transport or prolonged subaerial weathering.

Metamorphic lithic fragments (Lmm) are rare within the majority of the samples, but do occur with a high abundance within the forearc core (GeoB9816) near the Chile Triple Junction. The low-grade metamorphic rock fragments exhibit a characteristic platy shape as a result of a prominent schistosity and are often opaque (Fig. 7d). Sedimentary lithic fragments (Ls) are very rare, although some disintegration and loss during

sieving cannot be ruled out. Plutonic rock fragments almost exclusively occur in the southernmost samples. They mainly consist of quartz, feldspar and biotite, and probably relate to igneous rocks of the Patagonian Batholith on land. Bioclastic debris consisting of foraminifers and radiolarians is present as a minor constituent in most samples.

In the standard QFL diagram used for tectonic provenance analysis (e.g. Dickinson & Suczek 1979) most of the samples plot in one of the 'arc' fields (Fig. 8a). The trench fan turbidites and those from core GeoB9801, taken in the trench at 36°S, all plot in the undissected and transitional arc fields. This reflects the abundant influx of volcanic material into the Southern Chile Trench between 36°S and 41°S, driven by well-developed and efficient river systems and widespread outcrops of young volcanic rocks in the catchment areas. Figure 8b shows that some of the trench fans contain turbidites that have distinct provenance signatures. For example, those from the Biobío fan are poorest in quartz, and, along with the observation regarding the fresh volcanic glass (see above), contain the strongest 'volcanic' provenance signal. The turbidites from the Imperial and Chacao fans are richer in quartz, probably as a result of more material coming from the Coastal Cordillera. Seaward of the Callecalle River, there are two trench fans at the outlets of submarine canyons, with slightly different signatures for lithic fragment contents.

Concerning the lithic fragments, the provenance signal from the trench samples indicating volcanic sources is very strong (Fig. 8c), especially north of 41°S. South of 41°S the volcanic centres of the Southern Volcanic Zone continue (Fig. 1), but transport of volcanic detritus seaward to the trench is in part inhibited by the barrier formed by Chiloé Island and the Chonos Archipelago further south (Fig. 1). The three types of volcanic fragments plot within a restricted area (Fig. 8d), close to the microlitic endmember (Lvml), which is indicative of an andesitic provenance of most of the volcanic debris, and consistent with the high ratio of plagioclase to total feldspar (see above).

Discussion

In this discussion we focus on two main aspects of the results of this study: (1) the role of the provenance area, and its magmatic, tectonic, and oceanographic signatures for the depositional system; (2) the potential role of the turbidites as proxies of seismicity in the Southern Chile subduction zone.

The role of the provenance area

By the provenance analysis of the sandy turbidites it is possible to develop a clear image of the source area on land and its recent geological evolution. Holocene and young volcanic rocks dominate the geological picture in the source area north of 41°S. South of this latitude volcanic edifices are present, but the direct sediment transport from the arc to the trench is interrupted by the Chiloé and the Chonos islands (Fig. 1). Thus, the large proportion of volcanic lithic fragments (Fig. 8c) everywhere in the study area, also in the south, documents the easy mobilization of large amounts of ash-fall present after each eruption as well as the fact that volcanic edifices on land are quickly eroded and transported to the sea, even in areas where the nearshore geology is dominated by metamorphic and plutonic rocks with a much longer time delay between formation and eventual uplift and denudation. This case can be made especially for the Southern Chile Trench, where trench-parallel sediment transport is northward, and any dilution of a provenance signal along the trench would be in this direction.

The importance of volcanoes in the source area being mirrored within the sediment sink has already been described by Yerino & Maynard (1984), who were first to study the petrography of modern marine sands from the Peru–Chile Trench. They found proximity to recent volcanoes as the principal controlling factor, and a decrease in lithic fragments and increase in quartz in areas without recent volcanism. However, they did not resolve small-scale variations, such as the dominance of metamorphic lithic fragments in the vicinity of the Chile Triple Junction described within this study. Marsaglia *et al*. (1995) found very similar compositions of Pleistocene and Pliocene sand samples from ODP141 drill-holes. We take the petrographic similarity between our uppermost Holocene samples and the Pleistocene to Pliocene sands from the Chile Triple Junction as an indication that deglaciation has not had a major influence on turbidite sand compositions north of 47°S. This is to be expected, however, as the northward extent of Plio-Pleistocene glaciation (e.g. Rabassa & Clapperton 1990) in the Patagonian Andes was essentially limited northward at the Taitao Peninsula at about 46°30'S.

If the quartz content, both in the turbidites (Figs 4b and 8a) and the hemipelagic sediments (Fig. 4a) is taken as a provenance proxy for metamorphic and plutonic basement rocks, then the northward dilution of this signal by the sediment influx from the Southern Volcanic Zone of the Andes is clearly visible. Quartz abundances in the hemipelagic sediments decrease gradually from up to 33% to around 10–15% at 41°S, and remain at this level further north. In the trench and incoming plate turbidites south of 41°S, quartz content is highly variable, with a total average content of about one-third (see Fig. 8a), a value that fairly closely corresponds to non-recycled granitic or granodioritic continental or magmatic arc crust, such as the Patagonian Batholith. Further north trench turbidite composition (e.g. in core GeoB9801) resembles those of the trench fan turbidites. Also, the hemipelagic sediment records the northward increasing influence of the volcanic arc as a source area by its higher magnetic susceptibility (Fig. 5a). This observed pattern is in line with findings by Thornburg & Kulm (1987*b*), who described a northward increase in the relative contribution of volcanic sources with respect to plutonic sources between latitudes 45°S and 33°S, ascribed to a decrease in glaciation and arc dissection at lower latitudes.

Northward sediment transport along the trench should, in principle, result in an increase of fine grain-size fractions at least in the hemipelagic sediment. This may be a valid first-order approach to understand sediment distribution patterns, although in more detail sediment transport has to be seen as resulting from a combination of advective and non-linear dispersive mechanisms (Rios *et al*. 2003). In Figure 9, the latitudinal variations of clay and fine silt contents are displayed for the trench, the trench fan and the incoming plate. Clay and fine silt contents do indeed show a northward increase in the trench hemipelagic sediments. This can be explained in several ways. First, Lamy *et al*. (1998) observed an increase in finer material with increasing water depth, particularly below the CCD. Sand-sized calcareous microfossils are removed by dissolution, passively increasing the fine fractions (Krissek *et al*. 1980). Second, material emanates from many submarine canyons along the continental slope. Upon entering the trench, the natural pathway of the turbidity currents to the west is rerouted to the north and sediment-charged bottom currents will follow the natural northward slope. This northward transport direction of sediment is also suggested by asymmetrical trench fan geometries (Thornburg *et al*. 1990; Völker *et al*.

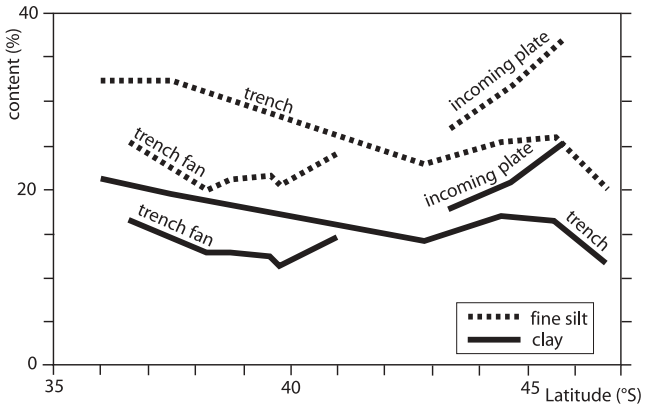

Fig. 9. Latitudinal grain-size variations depending on the setting of the sampling site. Northward increase of clay and fine silt content within the trench fill might be driven by greater water depths below the CCD in the north and thus dissolution of microfossils, by the general longitudinal northward transport and/or by coarser-grained source rocks in the south. Trends for trench fan and incoming plate sites are less pronounced, but grain-size distribution in the fans is more strongly dependent on the source area, and for the plate sites might be affected by currents.

2006). Third, coarser material at higher latitudes may be due to coarser-grained primary textures of the source rocks of the Patagonian Batholith area.

Fine fractions of the hemipelagic sediment from the trench fans do not show the same latitudinal variation (Fig. 9). This may be due to the trench fans being located directly at the mouths of submarine canyons, which are acting as point sources, and the grain-size distribution of the sediment offered being more directly dependent on the hydrology and geology of the onshore catchment areas.

In the hemipelagic sediment on the incoming plate, the clay and fine silt fractions become larger southward (Fig. 9). However, only three cores (GeoB9809, -10 and -13) were taken on the incoming plate and interpretation must be treated with caution. One possible scenario is that the southward-directed Peru–Chile Countercurrent may have affected sediment transport and resulting grain-size distribution patterns. However, variable proximity to the source area may be more important. In summary, it appears that the pattern of hemipelagic sediment distribution is affected by tectonics on the one hand, as the architecture of the Southern Chile Trench is directly related to the age of the Nazca Plate. On the other hand, currents may play an important role in defining the dispersal pattern of the fine-grained sediment.

The potential role of turbidites as seismic indicators

Attention will now be given to the potential role of the turbidites as a proxy of (mega-) seismicity in the Southern Chile subduction zone. Table 1 shows that frequencies of the documented turbidites are different for the three sample settings of the Nazca Plate, the trench and the trench fans. The trench fan sites show turbidite frequencies between 2.9 and 7.2 m^{-1} of core, whereas those within the trench range between 0.2 and 4.8 m^{-1}. The turbidite frequencies documented in the sections on the incoming plate are between zero and 1.1 m^{-1} of core. Total average frequencies are 4.6, 2.3 and 0.5 m^{-1} for the trench fans, trench and Nazca Plate, respectively. In principle, these differences are a proximity indicator, and can be easily understood in this context. We suppose that the most complete regional record of turbidites is to be found near the sediment source, at the trench fan sites. After estimating an average rate for hemipelagic background sedimentation, which accounts for most of the total sediment (see Table 1), the trench fan records will be used for comparison with data from the palaeoseismic record on land.

As direct isotopic or biostratigraphic age determinations on the cores are lacking, we estimate the age of the investigated sediments by a review of published age models from ODP drill-holes and piston cores as well as constraints imposed by the sediments found in the cores themselves. High sedimentation rates of 2.6 mm a^{-1} occur within the deepest parts of the Biobío canyon (Muñoz *et al*. 2004), illustrating the important role of the submarine canyons as major conduits of downslope particle transport, especially in areas with strong precipitation and high river discharges. However, such high rates are considered too high for the trench fans, where accumulation space widens and a high proportion of the sediment is diverted northward upon entering the trench. Sedimentation rates for ODP Site 1232, located at the outer rim of the trench at *c*. 40°S, and a gravity core (50SL) taken from an elevated seamount north of the Toltén canyon (Blumberg *et al*. 2008), not far away from Core GeoB9804, were found to be highly variable with respect to glacial and interglacial sediments: Holocene sedimentation rates are 0.1 mm a^{-1}, but corresponding rates were one order of magnitude higher during the Pleistocene. Because the samples at these sites were derived from distal and elevated locations with limited influx of terrigenous matter, these rates cannot directly be compared with those at our study sites. Sedimentation rates clustering around 2 mm a^{-1} were described for recent shelf and slope sediments off Concepción and Chiloé (Muñoz *et al*. 2004).

Within the somewhat distal locations of ODP Site 1232 and 50SL, numerous glacial turbidites reach thicknesses of more than 20 cm, making up more than 25–30% of the measured vertical columns, whereas Holocene turbidite layers are only a few millimetres thick (Blumberg *et al*. 2008). Glacial turbidites from more proximal sites, such as trench fans, are expected to show greater thicknesses and account for an even larger percentage of material within the cores. However, turbidites from SO181 gravity cores do not show any downcore increase in thickness that could indicate the transition from lower glacial to upper post-glacial sedimentation. They display low average ($\leqslant$5 cm) and low maximum (*c*. 10 cm) thicknesses, and generally make up less than 20% of the sediment column (Table 1). We thus conclude that our cores do not reach as far into the past as the last glacial period. This assumption is also corroborated by the absence of ice-rafted debris in all of the cores. Glacial dropstones have been documented at least in the southern part of the area in Pleistocene sediments cored during ODP Leg 141 (Behrmann *et al*. 1992).

As deglaciation of the Patagonian Andes is not yet fully understood (e.g. McCulloch *et al*. 2000; Kilian *et al*. 2007), possibly the best approximation comes from the work of Lamy *et al*. (2004), who suggested that changes in the Pleistocene extent of the Patagonian Ice Field had a 1000 year delayed response to changes in Pacific surface water temperatures at about 12 ka BP). This age is in line with the evolution of the Magellanic rainforest at about 11 ka BP (Fesq-Martin *et al*. 2004). Taking the hemipelagic section of the longest cores into account (644 mm, Table 1) approximate sedimentation rates over this time span would at least be 0.6 mm a^{-1} (644 mm in 11 ka). Without direct age control this average value is a rough estimate, which is largely dependent on both the penetration depth of the longest core as well as the precision of the underlying glacial–

interglacial transition. Taking earlier warming pulses into account, such as the transition from the Last Glacial Maximum to Termination I at *c*. 19 ka BP, for which Blumberg *et al*. (2008) noted a significant decrease in sedimentation rate, would significantly alter the sedimentation rate estimate. The uncertainty of the estimated rate is further increased by the fact that sedimentation rates were certainly not constant in time and space. However, the value of 0.6 mm a^{-1} fits well with respect to hemipelagic sedimentation rates of 0.08–0.43 mm a^{-1} for inter- and postglacial periods of the ODP Site 861 (Schönfeld *et al*. 1995) on the one hand and glacial sedimentation rates from the ODP Sites 1233 (2 mm a^{-1}), 1234 (0.8 mm a^{-1}) and 1235 (1 mm a^{-1}) (Mix *et al*. 2003; Stoner *et al*. 2008; for locations of ODP Sites see Fig. 1) on the other.

Accepting 0.6 mm a^{-1} as an approximate average sedimentation rate for the last 11 ka, the records from the trench fan cores can be used to constrain recurrence times for the turbidites. Estimates for mean intervals (arithmetic mean, median, maximum and minimum values) based on the inferred average sedimentation rate and the thickness of the interbedded hemipelagites are included in Table 1. Turbiditic layers occur fairly aperiodically, for part of which a variable background sedimentation rate might account. Generally, the majority of the clay layers (70–80%) between the turbidites vary in thickness by a factor of 2–3. However, a large spread in recurrence intervals agrees with observations from other palaeoseismic records that indicate a wide variance in time between subduction zone earthquakes (e.g. Ando 1975; Kelsey *et al*. 1998, 2002). Average recurrence intervals for the Biobío trench fan are 218 ± 117 years. For the Imperial trench fan this value is 192 ± 146 years. Because of the short core length of GeoB9805, the low number of turbiditic layers and one very thick hemipelagic interval the inferred recurrence intervals for the Toltén fan show a very large spread (327 ± 346 years). Highly variable recurrence intervals also apply for GeoB9806 from the Callecalle trench fan, with an estimated value of 334 ± 338 years. The second core from this trench fan (GeoB9807) yields an average rate of 477 ± 274 years. Turbiditic layers from the Chacao fan give an estimated flow periodicity of 240 ± 105 years.

The range of estimated turbidite recurrence rates fits well with data from published palaeoseismological records on land. The record from uplifted beach berms on Santa Maria Island at the northern end of the study area (Bookhagen *et al*. 2006) shows an average earthquake recurrence time of 180 ± 65 years for the last 3000 years. This is compatible with the turbidite recurrence time of 218 ± 117 years on the Biobío trench fan in the north of the investigated area. Further south, Nelson & Manley (1992) reconstructed a 300 year average recurrence time of earthquakes from uplifted beach berms on Isla Mocha, where 18 strandlines were preserved within 6000 years. Isla Mocha is immediately landward from the Imperial trench fan with an estimated turbidite recurrence time of 192 ± 146 years. Cisternas *et al*. (2005) estimated earthquake recurrence times of 285 years from sequences of sand-buried soils resulting from coseismic subsidence and tsunami flooding at Rio Maullín for the last 2000 years. Rio Maullín is closest to the Chacao trench fan site with an estimated turbidite recurrence time of 240 ± 105 years.

The relatively short historical record from the Valdivia earthquake rupture zone (Lomnitz 2004) shows earthquake recurrence times of about 130 years, and cannot be directly linked to turbidite recurrence. However, a recently published dated record of mass-wasting events in Lago Puyehue, landward from the Valdivia and Osorno districts (Moernaut *et al*. 2007) documents a temporal link to very large earthquakes in the Valdivia area in AD 1960, AD 1575 and 1660 cal years BP. Tentatively, these very large events could be recorded in the Callecalle and Toltén trench fan turbidites with recurrence intervals around 300–500 years (Table 1). Blumberg *et al*. (2008) deduced a Holocene turbidite recurrence rate of 1 ka, which differs greatly from the palaeoseismic record onland and the data presented herein. As mentioned above, only few flows have sufficient volume or velocity to reach such distal and elevated sites, and thus the record may be too patchy to warrant straightforward interpretation in terms of palaeoseismicity.

Not every turbidite is necessarily a seismoturbidite (Mutti *et al*. 1984), although the Holocene turbidite record from the Cascadia subduction zone, for example, was shown to be caused predominantly by seismic triggering (Adams 1990; Goldfinger *et al*. 2008). However, storms or sediment loading may add to the turbidite record. Additionally, the distribution of turbiditic deposits is patchy and governed by inherited erosional bedforms, and none of the sites records each turbidity current (e.g. Huh *et al*. 2006). For example, only cores GeoB9807 and GeoB9808, located just offshore Valdivia on the Callecalle fan and further to the south on the Chacao fan (Fig. 1), show a turbiditic layer just below the core top, for which we tentatively infer deposition following the great 1960 Valdivia earthquake (Mw = 9.5). Thus, even such strong ground shaking as during the 1960 event may remain unnoticed in the turbiditic records of the other submarine canyons. Comparison of palaeoseismic records off- and onshore is additionally fraught with difficulty as different approaches have variable threshold levels. Although our interpretation therefore needs to be considered with caution, inferred turbidite recurrence times in the Southern Chile Trench fans may indeed be broadly related to seismicity, on the basis of the large-scale rate estimates for Holocene sedimentation and the wide variance in estimated recurrence intervals. Some smaller, regional-scale links apparently exist between the palaeoseismic record on land and turbidite deposition in the trench fans. Here, high-resolution dating of the cores described in this study would be needed to provide further precision.

Conclusions

(1) Provenance analysis of sandy turbidites and the bulk mineralogical composition of the hemipelagic sediments from the cored material reflect onland geology on a regional scale. The hemipelagic sediment is clayey silt. In the south, the Patagonian Batholith constrains sediment composition. In the north, the detritus from the Andean volcanic arc is dominant. Plagioclase and quartz are the main constituents, and there is a strong southward increase of quartz content.

(2) A strong denudation signal from the volcanic rocks of the Southern Volcanic Zone of the Andes is documented in the amount of the lithic fragments. They reflect the high rate of destruction of the volcanic edifices on land, as opposed to the much slower denudation of the metamorphic and magmatic rocks in the Coastal Cordillera and the Patagonian Batholith area.

(3) The architecture of the Southern Chile Trench and the pattern of ocean currents have a profound influence on the size distribution of hemipelagic sediment. In the trench hemipelagic sediment becomes finer northward. On the Nazca Plate, this trend is reversed.

(4) Recurrence rates of sandy and silty turbidites in the trench fan sediments indicate a close connection to the palaeoseismic record on land. Our study documents the potential usefulness of proximal turbidites to reconstruct palaeoseismicity, even at the scale of single segments of the plate boundary. Such a recon-

struction, however, needs to be substantiated by high-resolution dating of the cores.

Our work was funded by the German Ministry of Education and Research (BMBF) under Grant No. 03G0594G to J.H.B. We are grateful for many discussions with members of the TIPTEQ working group. The assistance of scientists and marine crew of R.V. *Sonne* Expedition 181 was instrumental in the coring programme at sea, and is gratefully acknowledged. We thank D. Voelker and reviewers M. de Batist and J. Diaz Naveas for helpful suggestions and detailed criticism leading to significant improvements of the manuscript.

References

Adams, J. 1990. Paleoseismicity of the Cascadia subduction zone: evidence from turbidites off the Oregon–Washington margin. *Tectonics*, **9**, 569–583.

Aguirre, L., Hervé, A.F. & Godoy, P.B.E. 1972. Distribution of metamorphic facies in Chile; an outline. *Krystallinikum*, **9**, 7–19.

Ando, M. 1975. Source mechanisms and tectonic significance of historical earthquakes along the Nankai trough, Japan. *Tectonophysics*, **27**, 119–140.

Angermann, D., Klotz, J. & Reigber, C. 1999. Space–geodetic estimation of the Nazca–South America Euler vector. *Earth and Planetary Science Letters*, **171**, 329–334.

Bangs, N.L., Taira, A., Kuramoto, S., *et al.* 1999. U.S.–Japan Collaborative 3-D seismic investigation of the Nankai Trough plate-boundary interface and shallowmost seismogenic zone. *EOS Transactions, American Geophysical Union*, **80**, 569.

Behrmann, J.H. & Kopf, A. 2001. Balance of tectonically accreted and subducted sediment at the Chile Triple Junction. *International Journal of Earth Sciences*, **90**, 753–768.

Behrmann, J.H., Lewis, S.D.H., *et al.* eds) 1992. *Proceedings of the Ocean Drilling Program, Scientific Results, Initial Reports, 141*. Ocean Drilling Program. College Station, TX.

Behrmann, J.H., Lewis, S.D., Cande, S. & ODP Leg 141 Scientific Party 1994. Tectonics and geology of spreading ridge subduction at the Chile Triple Junction; a synthesis of results from Leg 141 of the Ocean Drilling Program. *Geologische Rundschau*, **83**, 832–852.

Blumberg, S., Lamy, F., Arz, H.W., Echtler, H.P., Wiedicke, M., Haug, G.H. & Oncken, O. 2008. Turbiditic trench deposits at the South-Chilean active margin: A Pleistocene–Holocene record of climate and tectonics. *Earth and Planetary Science Letters*, **268**, 526–539.

Boltovskoy, E. 1976. Distribution of Recent foraminifera of the South American region. *In:* Hedley, R.H. & Adams, C.G. (eds) *Foraminifera*. Academic Press, New York, 171–236.

Bookhagen, B., Echtler, H.P., Melnick, D., Strecker, M.R. & Spencer, J.Q.G. 2006. Using uplifted Holocene beach berms for paleoseismic analysis on the Santa María Island, south–central Chile. *Geophysical Research Letters*, **33**, L15302.

Cisternas, M., Atwater, B.F., Torrejon, F., *et al.* 2005. Predecessors of the giant 1960 Chile earthquake. *Nature*, **437**, 404–407.

DeMets, C., Gordon, R.G., Argus, D.F. & Stein, S. 1990. Current plate motions. *Geophysical Journal International*, **101**, 425–478.

Dickinson, W.R. 1970. Interpreting detrital modes of graywacke and arkose. *Journal of Sedimentary Petrology*, **40**, 695–707.

Dickinson, W.R. & Suczek, C.A. 1979. Plate tectonics and sandstone compositions. *AAPG Bulletin*, **63**, 2164–2182.

Fesq-Martin, M., Friedmann, A., Peters, M., Behrmann, J. & Kilian, R. 2004. Late Glacial and Holocene vegetation dynamics of the Magellanic rain forest in southern Patagonia, Chile. *Archaeobotany and Vegetation History*, **13**, 249–255.

Flüh, E. & Grevemeyer, I. 2005. *FS* Sonne *Fahrtbericht SO 181 TIPTEQ from the Incoming Plate to Megathrust Earthquakes*. IFM—Geomar Report, **2**.

Galli-Olivier, C. 1969. Climate, a primary control of sedimentation in the Peru–Chile Trench. *Geological Society of America Bulletin*, **80**, 1849–1852.

Goldfinger, C., Morey, A.E., Nelson, C.H., *et al.* 2007. Rupture lengths and temporal history of significant earthquakes on the offshore and north coast segments of the Northern San Andreas Fault based on turbidite stratigraphy. *Earth and Planetary Science Letters*, **254**, 9–27.

Goldfinger, C., Grijalva, K., Burgmann, R., *et al.* 2008. Late Holocene rupture of the northern San Andreas fault and possible stress linkage to the Cascadia subduction zone. *Bulletin of the Seismological Society of America*, **98**, 861–889.

Harbers, A. 2005. *Geotechnische Charakterisierung mariner Sedimente am südchilenischen Kontinentalrand: Auswertung der Expedition 181 der R/V* Sonne. Diplomarbeit, University of Bremen.

Hebbeln, D. & Cruise Participants 2001. *PUCK: Report and preliminary results of R/V* Sonne *Cruise SO156, Valparaiso (Chile)–Talcahuano (Chile), March 29–May 14, 2001*. Berichte aus dem Fachbereich Geowissenschaften der Universität Bremen, **182**.

Hebbeln, D., Lamy, F., Mohtadi, M. & Echtler, H. 2007. Tracing the impact of glacial–interglacial climate variability on erosion of the southern Andes. *Geology*, **35**, 131–134.

Heberer, B. 2008. *Tracking the provenance—Assessing sedimentary pathways and upper plate dynamics at the Chilean continental margin (29°–47°S)*. Doctoral thesis, University of Freiburg.

Huh, C.-A., Su, C.-C., Liang, W.-T. & Ling, C.-Y. 2004. Linkages between turbidites in the southern Okinawa Trough and submarine earthquakes. *Geophysical Research Letters*, **31**, L12304.

Huh, C.A., Su, C.C., Wang, C.H., Lee, S.Y. & Lin, I.T. 2006. Sedimentation in the Southern Okinawa Trough—Rates, turbidites and a sediment budget. *Marine Geology*, **231**, 129–139.

Kelsey, H.M., Witter, R.C. & Hemphill-Haley, E. 1998. Response of a small Oregon estuary to coseismic subsidence and postseismic uplift in the past 300 years. *Geology*, **26**, 231–234.

Kelsey, H.M., Witter, R.C. & Hemphill-Haley, E. 2002. Plate-boundary earthquakes and tsunamis of the past 5500 yr, Sixes River estuary, southern Oregon. *Geological Society of America Bulletin*, **114**, 298–314.

Kendrick, E., Bevis, M., Smalley, R.J., Brooks, B., Barriga, V.R., Lauria, E. & Fortes, L.P.S. 2003. The Nazca–South America Euler vector and its rate of change. *Journal of South American Earth Sciences*, **16**, 125–131.

Kilian, R. & Behrmann, J.H. 2003. Geochemical constraints on the sources of continent-related deep-sea sediments and their recycling in arc magmas of the Southern Andes. *Journal of the Geological Society, London*, **160**, 57–70.

Kilian, R., Schneider, Ch., Koch, J., *et al.* 2007. Paleoecological constraints on Late Glacial to Holocene ice retreat in the Southern Andes (53°S). *Global and Planetary Change*, **59**, 49–66.

Krissek, L.A., Scheidegger, K.F. & Kulm, L.D. 1980. Surface sediments of the Peru–Chile continental margin and the Nazca Plate. *Geological Society of America Bulletin*, **91**, 321–331.

Lamy, F., Hebbeln, D. & Wefer, G. 1998. Terrigenous sediment supply along the Chilean continental margin; modern regional patterns of texture and composition. *Geologische Rundschau*, **87**, 477–494.

Lamy, F., Hebbeln, D., Roehl, U. & Wefer, G. 2001. Holocene rainfall variability in southern Chile: a marine record of latitudinal shifts of the Southern Westerlies. *Earth and Planetary Science Letters*, **185**, 369–382.

Lamy, F., Kaiser, J., Ninnemann, U., Hebbeln, D., Arz, H.W. & Stoner, J. 2004. Antarctic timing of surface water changes off Chile and Patagonian Ice Sheet response. *Science*, **304**, 1959–1962.

Laursen, J. & Normark, W.R. 2002. Late Quaternary evolution of the San Antonio submarine canyon in the central Chile forearc (approximately 33° S). *Marine Geology*, **188**, 365–390.

LeRoux, J.P. & Elgueta, S. 2000. Sedimentologic development of a late Oligocene–Miocene forearc embayment, Valdivia Basin Complex, southern Chile. *Sedimentary Geology*, **130**, 27–44.

Lindquist, K.G., Engle, K., Stahlke, D. & Price, E. 2004. Global topography and bathymetry grid improves research efforts. *EOS Transactions, American Geophysical Union*, **85**, 186.

Link, O., Cecioni, A., Duyvestein, A. & Vargas, J. 2002. Hydrology of the Bio Bio River. *Zeitschrift fuer Geomorphologie Neue Folge, Supplementband*, **129**, 31–39.

Lomnitz, C. 2004. Major Earthquakes of Chile: A Historical Survey, 1535–1960. *Seismological Research Letters*, **75**, 368–378.

Marsaglia, K.M. & Tazaki, K. 1992. Diagenetic trends in Leg 126 sandstones. *In:* Taylor, B., Fujioka, K. & Janecek, T.R. (eds) *Proceedings of the Ocean Drilling Program, Scientific Results, 126*. Ocean Drilling Program, College Station, TX, 125–138.

Marsaglia, K.M., Torrez, X.V., Padilla, I. & Rimkus, K.C. 1995. Provenance of Pleistocene and Pliocene sand and sandstone, ODP Leg 141, Chile margin. *In:* Lewis, S.D., Behrmann, J.H., Musgrave, R.J. & Cande, S.C. (eds) *Proceedings of the Ocean Drilling Program, Scientific Results, 141*. Ocean Drilling Program, College Station, TX, 133–151.

Martin, M.W., Kato, T.T., Rodríguez, C., Godoy, E., Duhart, P., McDonough, M. & Campos, A. 1999. Evolution of the late Palaeozoic accretionary complex and overlying forearc–magmatic arc, south central Chile (38°–41°S): constraints for the tectonic setting along the south-western margin of Gondwana. *Tectonics*, **18**, 582–605.

McCulloch, R.D., Bentley, M.J., Purves, R.S., Hulton, N.R.J., Sugden, D.E. & Clapperton, C.M. 2000. Climatic inferences from glacial and palaeoecological evidence at the last glacial termination, southern South America. *Journal of Quaternary Science*, **15**, 409–417.

Melnick, D. & Echtler, H. 2006. Morphotectonic and geologic map compilations of the south–central Andes (36°–42°S). *In:* Oncken, O., Chong, G., Franz, G., *et al.* (eds) *The Andes: Active Subduction Orogeny*. Springer, Berlin, 565–568.

Mix, A.C., Tiedemann, R., Blum, P., *et al.* eds) 2003. *Proceedings of the Ocean Drilling Program, Initial Reports, 202*. Ocean Drilling Program, College Station, TX.

Moernaut, J., De Batist, M., Chartlet, F., *et al.* 2007. Giant earthquakes in South Central Chile revealed by Holocene mass wasting events in Lake Puyehue. *Sedimentary Geology*, **195**, 239–256.

Moerz, T. & Wolf-Welling, T.C.W. 2002. Fine-fraction grain-size distribution data and their statistical treatment and relation to processes, Site 1095 (ODP Leg 178, western Antarctic Peninsula). *In:* Barker, P.F., Camerlenghi, A., Acton, G.D. & Ramsay, A.T.S. (eds) *Proceedings of the Ocean Drilling Program, Scientific Results, 178*. Ocean Drilling Program, College Station, TX, 1–27.

Moreno, T. & Gibbons, W. 2007. *The Geology of Chile*. Geological Society, London.

Muñoz, P., Lange, C.B., Gutiérrez, D., *et al.* 2004. Recent sedimentation and mass accumulation rates based on ^{210}Pb along the Peru–Chile continental margin. *Deep-Sea Research II*, **51**, 2523–2541.

Mutti, E., Lucchi, F. R., Seguret, M. & Zanzucchi, G. 1984. Seismoturbidites: A new group of resedimented deposits. *Marine Geology*, **55**, 103–116.

Nelson, A.R. & Manley, W.F. 1992. Holocene coseismic and aseismic uplift of Isla Mocha, south–central Chile. *Quaternary International*, **15–16**, 61–76.

Pankhurst, R.J. & Hervé, F. 2007. Introduction and overview. *In:* Moreno, T. & Gibbons, W. (eds) *The Geology of Chile*. Geological Society, London, 1–4.

Rabassa, J. & Clapperton, C. 1990. Quaternary glaciations of the southern Andes. *Quaternary Science Reviews*, **9**, 153–174.

Ramos, V.A. & Kay, S.M. 1992. Southern Patagonia plateau basalts and deformation: back arc testimony of ridge collision. *Tectonophysics*, **205**, 79–91.

Ranero, C.R., von Huene, R., Weinrebe, W. & Reichert, C. 2006. Tectonic processes along the Chile convergent margin. *In:* Oncken, O., Chong, G., Franz, G., *et al.* (eds) *The Andes: Active Subduction Orogeny.* Springer, Berlin, 91–121.

Rietveld, H.M. 1969. A profile refinement method for nuclear and magnetic structures. *Journal of Applied Crystallography*, **2**, 65–71.

Rios, F., Ulloa, R. & Corream, I.C.S. 2003. Determination of net sediment transport patterns in Lirquen Harbor, Chile, through grain-size trend analysis; a test of methods. *Pesquisas em Geociencias*, **30**, 65–81.

Röser, G. 2007. *Petrography, physical properties, and geotechnical behavior of modern sediments, Southern Chile Trench*. Doctoral thesis, University of Freiburg.

Schmincke, H.U. 1982. Ash from vitric muds in deep sea cores from the Mariana Trough and fore-arc region (South Philippine Sea) (Sites 453,454, 455, 458, 459, and SP), Deep Sea Drilling Project Leg 60. *In:* Lee, M., Powell, R., Hussong Donald, M. & Uyeda, S. (eds) *Initial Reports of the Deep Sea Drilling Project, 60*. US Government Printing Office, Washington, DC, 473–481.

Scholl, D.W., Christensen, M.N., von Huene, R. & Marlow, M.S. 1970. Peru–Chile Trench sediments and sea-floor spreading. *Geological Society of America Bulletin*, **81**, 1339–1360.

Schönfeld, J., Spiegler, D. & Erlenkeuser, H. 1995. Late Quaternary stable isotope record of planktonic and benthic foraminifers: Site 861, Chile Triple Junction, Southeastern Pacific. *In:* Lewis, S.D., Behrmann, J.H., Musgrave, R.J. & Cande, S.C. (eds) *Proceedings of the Ocean Drilling Program, Scientific Results, 141*. Ocean Drilling Program, College Station, TX, 235–240.

Schweller, W.J. & Kulm, L.D. 1978. Depositional patterns and channelized sedimentation in active eastern Pacific trenches. *In:* Stanley, D.J. & Kelling, G. (eds) *Sedimentation in Submarine Canyons, Fans, and Trenches*. Hutchinson & Ross, Stroudsburg, PA, 311–323.

SERNAGEOMIN 2003. *Geological map of Chile*, digital version, scale 1:1 000 000.

Sepúlveda, S.A., Rebolledo, S. & Vargas, G. 2006. Recent catastrophic debris flows in Chile: Geological hazard, climatic relationships and human response. *Quaternary International*, **158**, 83–95.

Shaffer, G., Salinas, S., Pizarro, O., Vega, A. & Hormazabal, S. 1995. Currents in the deep ocean off Chile (30°). *Deep-Sea Research*, **42**, 425–436.

Sick, C., Yoon, M.-K., Rauch, K., *et al.* 2006. Seismic images of accretive and erosive subduction zones from the Chile margin. *In:* Oncken, O., Chong, G., Franz, G., *et al.* (eds) *The Andes: Active Subduction Orogeny.* Springer, Berlin, 147–170.

Smith, W.H.F. & Sandwell, D.T. 1997. Global sea floor topography from satellite altimetry and ship depth soundings. *Nature*, **277**, 1956–1962.

Stoner, J.S., Lund, S., Channell, J.E., Mix, A.C., Davies, M.H. & Lamy, F. 2008. High sedimentation rate paleomagnetic records for the last 70 kyrs from the Chilean margin. American Geophysical Union, Fall Meeting 2008, abstract no. GP14A-02.

Strub, P.T., Mesias, J.M., Montecino, V., Rutlant, J. & Salinas, S. 1998. Coastal ocean circulation off Western South America. *In:* Robinson, A.R. & Brink, K.H. (eds) *The Global Coastal Ocean*. Wiley, Chichester, 273–314.

Tebbens, S.F. & Cande, S.C. 1997. Southeast Pacific tectonic evolution from early Oligocene to present. *Journal of Geophysical Research*, **102**, 12061–12084.

Thornburg, T.M. & Kulm, L.D. 1987*a*. Sedimentation in the Chile Trench: depositional morphologies, lithofacies, and stratigraphy. *Geological Society of America Bulletin*, **98**, 33–52.

Thornburg, T.M. & Kulm, L. D. 1987*b*. Sedimentation in the Chile Trench; petrofacies and provenance. *Journal of Sedimentary Research*, **57**, 55–74.

Thornburg, T.M., Kulm, L.D. & Hussong, D.M. 1990. Submarine-fan development in the southern Chile Trench; a dynamic interplay of tectonics and sedimentation. *Geological Society of America Bulletin*, **102**, 1658–1680.

Underwood, M.B. & Karig, D.E. 1980. Role of submarine canyons in trench and trench-slope sedimentation. *Geology*, **8**, 432–436.

Underwood, M.B., Orr, R., Pickering, K. & Taira, A. 1993. Provenance and dispersal patterns of sediments in the turbidite wedge of Nankai Trough. *In:* Hill, I.A., Taira, A., Firth, J.V., *et al.* (eds) *Proceedings of the Ocean Drilling Program, Scientific Results, 131*. Ocean Drilling Program, College Station, TX, 15–34.

Völker, D., Wiedicke, M., Ladage, S., *et al.* 2006. Latitudinal variation in sedimentary processes in the Peru–Chile Trench off Central Chile. *In:* Oncken, O., Chong, G., Franz, G., *et al.* (eds) *The Andes: Active Subduction Orogeny.* Springer, Berlin, 193–216.

Weber, M.E., Niessen, F., Kuhn, G. & Wiedicke, M. 1996. The multi-sensor core logger; a high-resolution tool to investigate marine sediments. *In:* Mienert, J. & Wefer, G. (eds) *International Congress on Coring for Global Change, ICGC '95*. GEOMAR Report, **45**, 67–68.

Weber, M.E., Niessen, F., Kuhn, G. & Wiedicke, M. 1997. Calibration and application of marine sedimentary physical properties using a multi-sensor core logger. *Marine Geology*, **136**, 151–172.

Willner, A.P., Hervé, F. & Massonne, H.J. 2000. Mineral chemistry and pressure–temperature evolution of two contrasting high-pressure–low-temperature belts in the Chonos Archipelago, southern Chile. *Journal of Petrology*, **41**, 309–330.

Yañez, G., Cembrano, J., Pardo, M., Ranero, C. & Selles, D. 2002. The Challenger–Juan Fernandez–Maipo major tectonic transition of the Nazca–Andean subduction system at 33–34°S; geodynamic evidence and implications. *Journal of South American Earth Sciences*, **15**, 23–38.

Yerino, L.N. & Maynard, J.B. 1984. Petrography of modern marine sands from the Peru–Chile Trench and adjacent areas. *Sedimentology*, **31**, 83–89.

Zapata, R.A. 2001. *Estudio batimetrico del margen Chileno*. Departamento de Geofisica, Universidad de Chile, Santiago.

Received 10 February 2009; revised typescript accepted 8 December 2009.
Scientific editing by Gary Hampson.